Current Leakage and Faradaic Efficiency Simulation of Proton-Conducting Solid Oxide Electrolysis Cells

ECS Transactions, 111 (6) 1159-1167 (2023)
10.1149/11106.1159ecst ©The Electrochemical Society

Current Leakage and Faradaic Efficiency Simulation of Proton-Conducting Solid Oxide Electrolysis Cells

Yasser Shoukry[1] and Xinfang Jin[1]*

Mechanical Engineering Department, University of Massachusetts, Lowell, MA01854

*Corresponding author: Xinfang_Jin@uml.edu

Abstract

In this study, we simulated BZY electrolyte supported proton-conducting solid oxide cell by coupling surface defect chemistry reaction with charged species transport. We validated the model parameters by OH^g concentration as a function of temperature, conductivity under dry and wet oxygen as a function of oxygen partial pressure and temperature. The results indicate that the high electron hole mobility (diffusivity) is mainly responsible for the high leaking current under high temperature. The Faradaic efficiency stays low or even negative under low operating voltage or high temperature and plateaus as the cell voltage increases. The model developed in this study is a useful tool to understand the leaking current in BZY electrolyte and provide design strategies to avoid/mitigate such significant inefficiency for water electrolysis operation.

Keywords: BZY, Faradaic Efficiency, Leaking Current, Nernst-Planck

I. Introduction

Proton conducting solid oxide electrolysis cells (P-SOEC) have advantages over its oxygen-ion-conducting (O-SOEC) counterpart due to lower operating temperature (e.g. 300-700^{o}C), relatively lower activation energy, and easier gas separation [1, 2]. However, it suffers from low Faradaic efficiency led by the internal current leakage. Protonic ceramics like $BaZr_{0.90}Y_{0.10}O_3$ (BZY) are generally mixed proton, oxygen vacancy and electron hole conducting oxides, in which the transference number of each charge carrier depends on the material composition, operating temperature, atmosphere, and polarization current density. Experimental results have been reported that BZY shows significant p-type electronic leakage [3] across the electrolyte resulting in a flux of hydrogen from the negative electrode to the positive electrode and reducing the Faradaic efficiency. However, the fundamental understanding of the formation of electronic charge carriers during electrolysis operation is still unknown.

In this research, we simulate a P-SOEC with BZY electrolyte with defect chemistry and Nernst-Planck charge conservation [4] to couple thermodynamic equilibrium of both electrodes under polarized operating conditions. Three mobile charge carriers are considered in BZY electrolyte, including proton, oxide vacancy and electron hole, which is balanced with the dopant concentration Y'_{Zr} . The thermodynamic equilibrium is used to solve for charge species concentration in different gas atmosphere. The thermodynamic parameters are validated by

experimental data of BZY proton concentration [5] under different operating temperature and different O_2 or H_2O partial pressures. The mobility of each charged species are also validated by overall conductivity of BZY [6]. Then, the model is used to project internal electronic current leakage and Faradaic efficiency from open circuit voltage to Nernst potential and beyond. The correlation between Faradaic efficiency and operating current density is established to explain the experimental observations. Ultimately, the model could help establish strategies to minimize electronic leakage by tailoring the composition of the electrolyte, optimizing device architecture, and manipulating P-SOEC operating conditions.

II. Mathematical Model

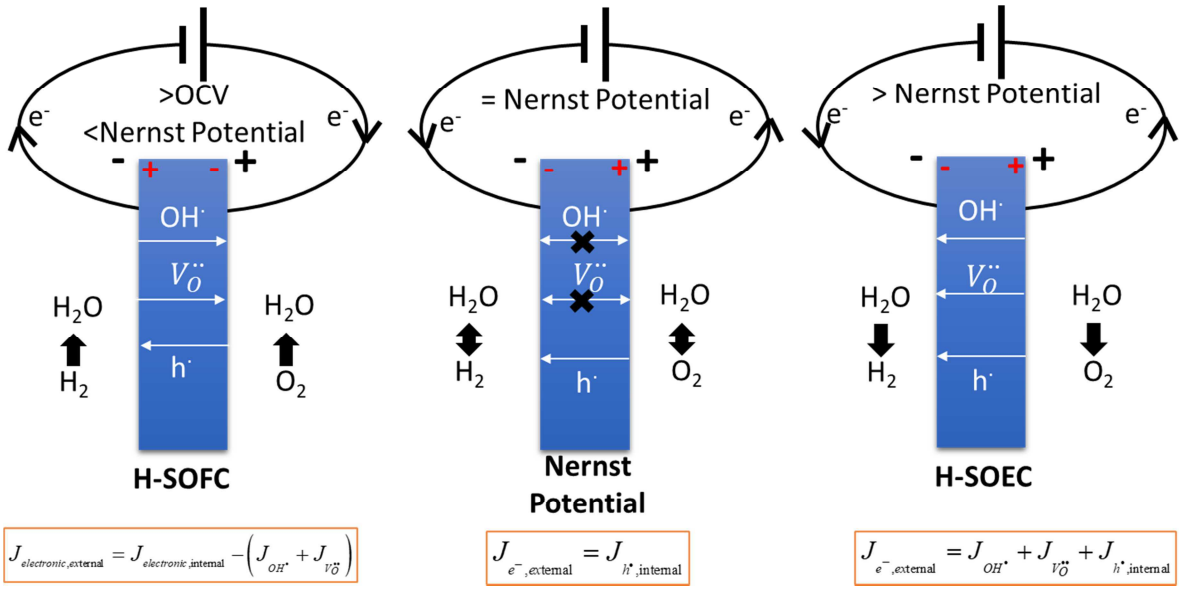

Fig 1. Current Conservation of Mixed Conducting P-SOEC Electrolyte Under Different Operating Voltages

P-SOECs have historically suffered from low Faradaic efficiencies, which is ascribed to electronic leakage caused by the mixed electronic conductivity of BZY electrolyte. To understand the current leakage mechanism, we are building a Multiphysics 1D model using Nernst-Planck equation to uncover how the charged species concentration and electronic potential could contribute to the leaking current. And also, we are understanding the problem starting from open circuit voltage (no external current, lower than Nernst potential in most conditions) to Nernst potential and then high current density for SOEC operation mode, as shown in Fig 1. The charged species in BZY electrolyte include: oxygen vacancy $V_O^{\cdot\cdot}$, proton $OH^{\cdot}$, and electron hole $h^{\cdot}$. Their concentrations are determined based on the thermodynamic equilibrium between the solid phase and gas phase. The electronic potential will be generated either to counter the concentration gradient or to respond to the external potential. There are three stages of P-Solid Oxide Cell (P-SOC) operation: 1) the cell potential across the electrolyte is in between the Open Circuit Voltage and Nernst Potential. Under such an operating condition, because of current leakage caused by concentration gradient of charged species, the solid oxide

cell is still operating under pseudo-SOFC mode, in which it consumes H_2 and O_2 to generate H_2O. The external electronic current is less than the internal leaking current. 2) As the cell voltage increases to Nernst Potential, the electronic potential becomes stronger and is able to counter the concentration gradient caused ionic flux in the opposite direction. So the ionic flux from oxygen vacancy and proton become 0. The external electronic current becomes the same as the internal leaking current. 3) As the cell voltage increases further, the flowing direction of oxygen vacancies and protons have been reversed. Therefore, the external current becomes the summation of the ionic current and electronic leaking current inside of the electrolyte.

The governing equations and boundary conditions for the BZY electrolyte supported P-SOEC have been listed in Table 1. The activation overpotentials of both electrodes are calculated from Bulter-Volmer equations using two Global ODEs:

$$i_{0,H_2}\left(\exp\left(\frac{\alpha ZF}{RT}\eta_{H_2}\right)-\exp\left(-\frac{\alpha ZF}{RT}\eta_{H_2}\right)\right)=current \tag{1}$$

$$i_{0,O_2}\left(\exp\left(\frac{\alpha ZF}{RT}\eta_{O_2}\right)-\exp\left(-\frac{\alpha ZF}{RT}\eta_{O_2}\right)\right)=current \tag{2}$$

Where i_0 is the exchange current density; $\eta=\phi_e-\phi_i-E_{eq}$ is the overpotential in each electrode; 'current' represents the external current density. And the subscript H_2 and O_2 refer to H_2 electrode and O_2 electrode respectively.

The electronic potential at H_2 electrode and O_2 electrode are calculated as:

$$\phi_{e,H_2}=-\eta_{H_2}+\phi_{i,BZY}+0[V] \tag{3}$$

$$\phi_{e,O_2}=\eta_{O_2}+\phi_{i,BZY}+E_{eq} \tag{4}$$

Here we assume that under SOEC mode, the external current density is positive, and it is negative under SOFC mode. The signs in front of activation overpotential have been defined accordingly. The overall cell voltage and Nernst potential are defined as shown below:

$$V_{cell}=\phi_{e,O_2}-\phi_{e,H_2} \tag{5}$$

$$E_{eq}=\frac{RT}{4F}\log\left(\frac{P_{O_2,O_2\text{ electrode}}}{P_{O_2,H_2\text{ electrode}}}\right) \tag{6}$$

Table 1: Governing equations and boundary conditions for an BZY electrolyte supported P-SOEC.

Dependent Variable	Governing Equation	BC (X = 0)	BC (X = L)
$C_{\mathrm{V_o^{\cdot\cdot}}}$	$\nabla \boldsymbol{J}_{V_o^{\cdot\cdot}} = -Z_{V_o^{\cdot\cdot}} F D_{V_o^{\cdot\cdot}} \nabla^2 C_{V_o^{\cdot\cdot}} - \frac{D_{V_o^{\cdot\cdot}} F^2 {Z_{V_o^{\cdot\cdot}}}^2}{RT} C_{V_o^{\cdot\cdot}} \nabla^2(\phi_{i,BZY})$	$\left(C_{V_O^{\cdot\cdot}}\right)_0$	$\left(C_{V_O^{\cdot\cdot}}\right)_L$
$C_{\mathrm{OH_o}}$	$\nabla \boldsymbol{J}_{\mathrm{OH_o}} = -Z_{\mathrm{OH_o}} F D_{\mathrm{OH_o}} \nabla^2 C_{\mathrm{OH_o}} - \frac{D_{\mathrm{OH_o}} F^2 {Z_{\mathrm{OH_o}}}^2}{RT} C_{\mathrm{OH_o}} \nabla^2(\phi_{i,BZY})$	$\left(C_{(OH)_O^{\cdot}}\right)_0$	$\left(C_{(OH)_O^{\cdot}}\right)_L$
$\phi_{i,BZY}$	$\nabla \boldsymbol{J}_{h^{\cdot}} = -Z_{h^{\cdot}} F D_{h^{\cdot}} \nabla^2(C_{h^{\cdot}}) - \frac{D_{h^{\cdot}} {Z_{h^{\cdot}}}^2 F^2}{RT} C_{h^{\cdot}} \nabla^2(\phi_{i,BZY})$	$\phi_{i,BZY} = 0$	Current-$\left(\boldsymbol{J}_{V_O^{\cdot\cdot}} \boldsymbol{J}_{\mathrm{OH_o}}\right)$
$C_{h^{\cdot}}$	$C_{h^{\cdot}} + C_{\mathrm{OH_o}} + 2C_{\mathrm{V_o^{\cdot\cdot}}} - C_{\mathrm{Y'_{Zr}}} = 0$	-	-

ECS Transactions, 111 (6) 1159-1167 (2023)

III. Parameters and Validation

Based on Kroger-Vink notation, the defect surface reactions have been reported previously by Kee's group [7]. Here we implemented the same defect chemistry model with extensive validation to identify thermodynamics and transport parameters for three major charge species: oxygen vacancy, proton, and electron hole. It has been confirmed that electron concentration is several orders of magnitude lower than electron hole or other ionic charge species and could be neglected.

For validation, five steps have been taken: 1) adjust ΔS^o for reaction 3 to fit mol % of proton concentration as a function of temperature between experimental data in Fig.2a from Kreuer [5] and model prediction. 2) adjust D_k^o and E_k for $V_O^{\bullet\bullet}$ to fit the plateau conductivity in Fig.2c [8] with model prediction. 3) adjust ΔH^o and ΔS^o for reaction 2 and D_k^o and E_k for $h^{\bullet}$ to fit the dramatic increase of conductivity under high oxygen partial pressure in Fig. 2c. 4) adjust D_k^o and E_k for $OH_O^{\bullet}$ to fit the plateau conductivity in Fig.2b [8] with model prediction. 5) adjust the parameters related to $h^{\bullet}$ and $OH_O^{\bullet}$ to ensure that the open circuit voltage is lower than Nerst potential. The comparison between model predictions (solid lines) and experimental data (symbols) in Fig.2 show good agreements among all three sets of data.

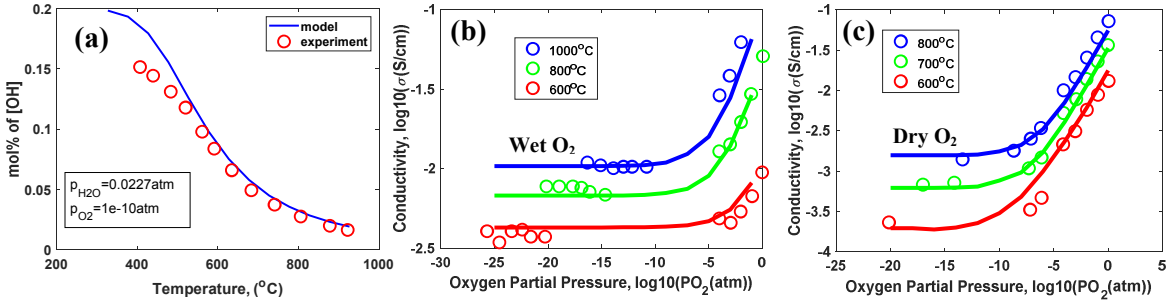

Fig 2. Model (solid lines) and experiment (symbols) comparison (a) [OH] mol % as a function of temperature (°C) under P_{H2O}=0.0227atm and P_{O2}=1e-10atm; Conductivity (S/cm), as a function of oxygen partial pressure (atm), (b) under wet O_2 condition;(c) under dry O_2

The thermodynamic equilibrium parameters and transport parameters for surface defect reactions are cited from Kee's paper [7] and adjusted for the validation purpose. The parameters used in this study are listed in Table 2 and Table 3.

Table 2 Thermodynamics for surface defect reactions.

Index	Reactions	ΔH^o (kJ mol^{-1})	ΔS^o (J mol^{-1} K^{-1})	Kp (750°C)
1	$\frac{1}{2}H_2 + O_o^X \leftrightarrow OH_O^{\bullet} + e^{'}$	164.35	-17.85	4.74×10^{-10}
2	$\frac{1}{2}O_2 + V_O^{\bullet\bullet} \leftrightarrow O_O^X + 2h^{\bullet}$	-135.0/-80*	-130.0/-120*	1.26
3	$H_2O + V_O^{\bullet\bullet} + O_O^X \leftrightarrow 2OH_O^{\bullet}$	-93.3	-113.2/-83.2*	7.09×10^{-2}
4	$null \leftrightarrow h^{\bullet} + e^{'}$	266.2	0	2.55×10^{-14}

5	$H_2 + \frac{1}{2}O_2 \leftrightarrow H_2O$	-245.45	-52.51	6.13×10^{9}

Note: the parameters with * are adjusted.

Table 3 Charged-defect diffusion coefficient, $D_k = D_k^0 \exp(E_k / RT)$.

Charged defect	D_k^o **($m^2\ s^{-1}$)**	E_k **(kJ mol^{-1})**
$OH_O^{\bullet}$	1.55×10^{-8}	43.0
$V_O^{\bullet\bullet}$	$1.90\times10^{-9}/3.0\times10^{-7}$*	70.0/89*
$h^{\bullet}$	$1.05\times10^{-6}/4.0\times10^{-4}$*	97.0/90*
$e^{'}$	1.70×10^{-7}	90.0

Note: the parameters with * are adjusted.

IV. Results and Discussion

After validation, the model has been used to study the effect of temperature and current density on cell performance. P-SOEC has been known as an electrochemical device suited for intermediate temperature operation. Therefore, the operating range is varied between 500°C and 750°C. The current density operating range varies from -0.1 A/cm^2 (SOFC mode) to 2A/cm^2 (SOEC mode). In this section, we will illustrate how the leaking electronic current will be impacted by current density and temperature.

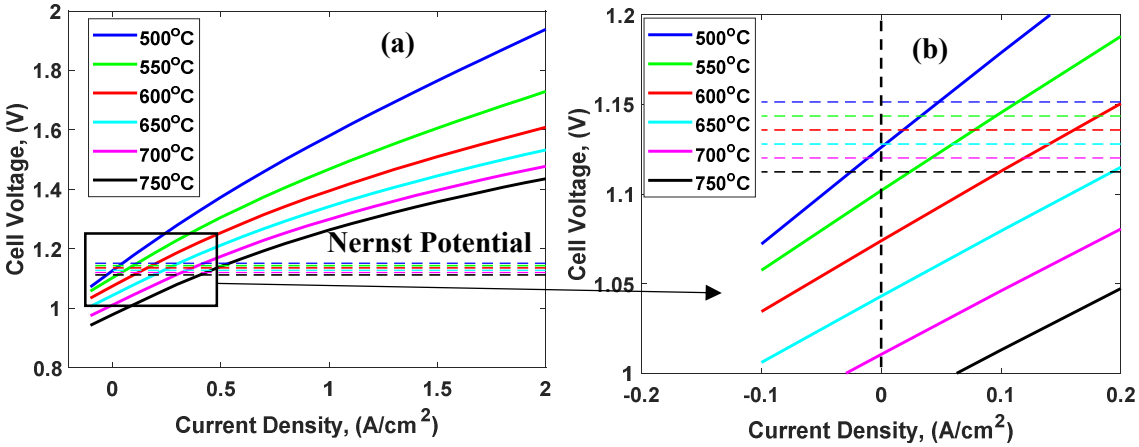

Fig 3. Cell Voltage as a function of current density under different temperatures (a) Full current density range; (b) Enlarged plot close to open circuit voltage. Note: horizontal lines are Nernst potentials under each corresponding temperature.

In Fig.3, the horizontal dashed lines represent the Nernst potential under certain temperatures; the solid lines show the cell voltage under different temperatures. For BZY material, because of internal leaking current, the open circuit voltage (OCV), under which external current density is 0, is generally lower than its corresponding Nernst Potential. Fig.3b shows an enlarged plot around open circuit voltage. It illustrates that under low temperature, e. g. 500°C, OCV is only

30mV lower than its Nernst potential; whereas as temperature increases to 700°C, the difference is more than 100mV, indicating a much higher leaking current under higher temperature. Another fact from Fig. 3b is that as the temperature increases, the Nernst potential decreases, which is consistent with thermodynamic parameters listed in Table 2 for reaction 5. From Fig. 3a, we could also observe that the cell voltage under the same current density is much higher under low temperature. Such an increase in cell voltage is mainly resulted from solid/gas interface equilibrium and transport properties variation under different temperatures. Electrode polarization is not the focus of the study, so the exchange current density has been assumed to be a constant.

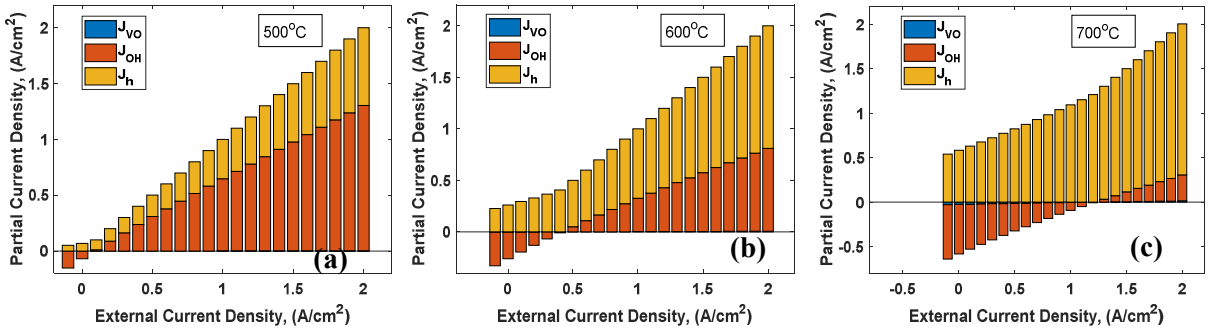

Fig 4. Partial current density variation as the external current density increases from -0.1 A/cm^2 (SOFC) to 2 A/cm^2 (SOEC). (a) under 500°C, (b) under 600°C;(c) under 700°C.

Since BZY electrolyte is a mixed conductor, which will be impacted significantly by the operating conditions, we also plotted the partial current density contribution from different charged species, including oxygen vacancy $V_O^{\bullet\bullet}$, proton OH^g, and electron hole h^g. As shown in Fig. 4, $V_O^{\bullet\bullet}$ has a negligible contribution to the overall current density. Under 500°C, OH^g dominates the overall current in the electrolyte. As the temperature increases, h^g becomes the dominant charged species and counts for most of the external current density. Therefore, as temperature increases, current leakage problem worsens. In addition, we could also observe that under open circuit voltage, the leaking current is balanced by OH^g current in the opposite direction to realize 0 external current density.

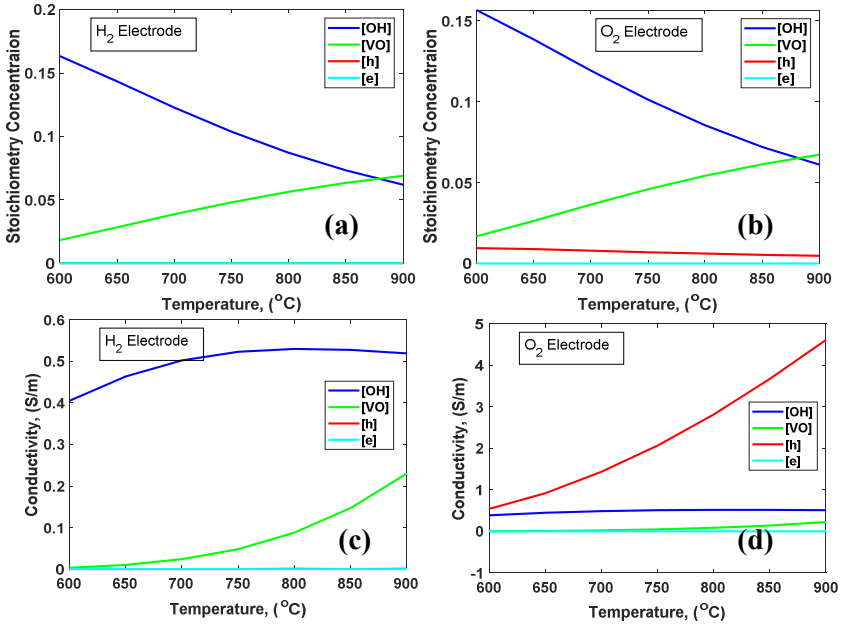

Fig 5. As a function of temperature, Variation of stoichiometry concentration of charged species, (a) at H_2 electrode side, (b) at O_2 electrode side; Variation of Conductivity, (c) at H_2 electrode side, (d) at O_2 electrode side.

Since the high leaking current could be caused by two factors: high electron hole concentration or high electron hole diffusivity. In Fig.5, it is illustrated that the stoichiometry concentration and conductivity variation in each electrode/electrolyte interface as a function of temperature. It is found that the electronic conductivity is rooted in the O_2 electrode/electrolyte interface with high electron hole diffusivity rather than high electron hole concentration. Many research suggests that in BZY, proton diffusivity could surpass that of the electron hole. Based on our model, if that happens, the open circuit voltage will become higher than Nernst potential, which is contradicted with experimental observation. Therefore, we conclude that the high leaking current in BZY is caused by high electron hole diffusivity rather than high concentration of electron hole.

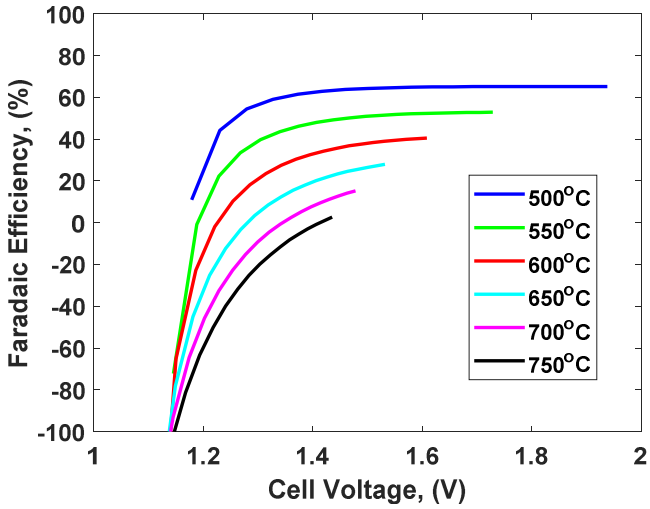

Fig 6. Faradaic efficiency (%) as a function of cell voltage (V) under different temperatures.

We finally plotted the Faradaic Efficiency of the cell under different cell voltages and temperatures in Fig. 6. Under 500°C, the Faradaic efficiency is increasing gradually as the cell voltage increases and eventually it plateaus out around 70%. As temperature increases, current leakage will be enhanced. Therefore, Faradaic efficiency could stay negative under lower voltage. As cell voltage continues to increase, Faradaic efficiency reaches a new plateau at a much lower value. Negative efficiency indicates that there is no water splitting reaction and on the contrary, there is continuous consumption of H_2 and O_2. Fig.6 shows similar trends with that reported in the literature from experiment. The model developed in this study could help us have a better understanding of leaking current in BZY electrolyte and provide design strategies to avoid/mitigate such significant inefficiency for water electrolysis operation.

V. Conclusion

In this study, we coupled surface defect chemistry reaction with charged species transport in mixed conducting proton conducting BZY electrolyte. The model parameters have been properly validated by OH^g concentration as a function of temperature, conductivity under dry and wet oxygen as a function of oxygen partial pressure and temperature. The results indicate that the high electron hole mobility (diffusivity) is mainly responsible for the high leaking current under high temperature. The Faradaic efficiency stays low or even negative under low operating voltage and plateaus out as the cell voltage increases. The model developed in this study could help us have a better understanding of leaking current in BZY electrolyte and provide design strategies to avoid/mitigate such significant inefficiency for water electrolysis operation.

Acknowledgement

This material is based upon work supported by the U.S. National Science Foundation under grant number CBET-1924095.

References:

1. Duan, C., et al., *Proton-conducting oxides for energy conversion and storage.* Applied Physics Reviews, 2020. **7**(1): p. 011314.
2. Lei, L., et al., *Progress Report on Proton Conducting Solid Oxide Electrolysis Cells.* Advanced Functional Materials, 2019. **29**(37): p. 1903805.
3. Choi, S., T.C. Davenport, and S.M. Haile, *Protonic ceramic electrochemical cells for hydrogen production and electricity generation: exceptional reversibility, stability, and demonstrated faradaic efficiency.* Energy & Environmental Science, 2019. **12**(1): p. 206-215.
4. Duncan, K.L. and E.D. Wachsman, *Continuum-Level Analytical Model for Solid Oxide Fuel Cells with Mixed Conducting Electrolytes.* Journal of The Electrochemical Society, 2009. **156**(9): p. B1030.
5. Kreuer, K.D., et al., *Proton conducting alkaline earth zirconates and titanates for high drain electrochemical applications.* Solid State Ionics, 2001. **145**(1): p. 295-306.
6. Nomura, K. and H. Kageyama, *Transport properties of Ba(Zr0.8Y0.2)O3−δ perovskite.* Solid State Ionics, 2007. **178**(7): p. 661-665.
7. Robert J. Kee, Huayang Zhu, Brett W. Hildenbrand, Einar Vøllestad, Michael D. Sanders, and Ryan P. O'Hayre, *Modeling the Steady-State and Transient Response of Polarized and Non-Polarized Proton-Conducting Doped-Perovskite Membranes.* Journal of The Electrochemical Society, 160 (3) F290-F300 (2013).
8. Katsuhiro Nomura, Hiroyuki Kageyama, Transport properties of Ba(Zr0.8Y0.2)O3−δ perovskite, Solid State Ionics, Volume 178, Issues 7–10, 2007, Pages 661-665, https://doi.org/10.1016/j.ssi.2007.02.010.